

# FUSION: Full-Body Unified Motion Prior for Body and Hands via Diffusion

Enes Duran<sup>1,2</sup> Nikos Athanasiou<sup>1</sup> Muhammed Kocabas<sup>3</sup> Michael J. Black<sup>1</sup>  
Omid Taheri<sup>1</sup>

<sup>1</sup> Max Planck Institute for Intelligent Systems, <sup>2</sup> University of Tübingen <sup>3</sup> Meshcapade GmbH, Germany

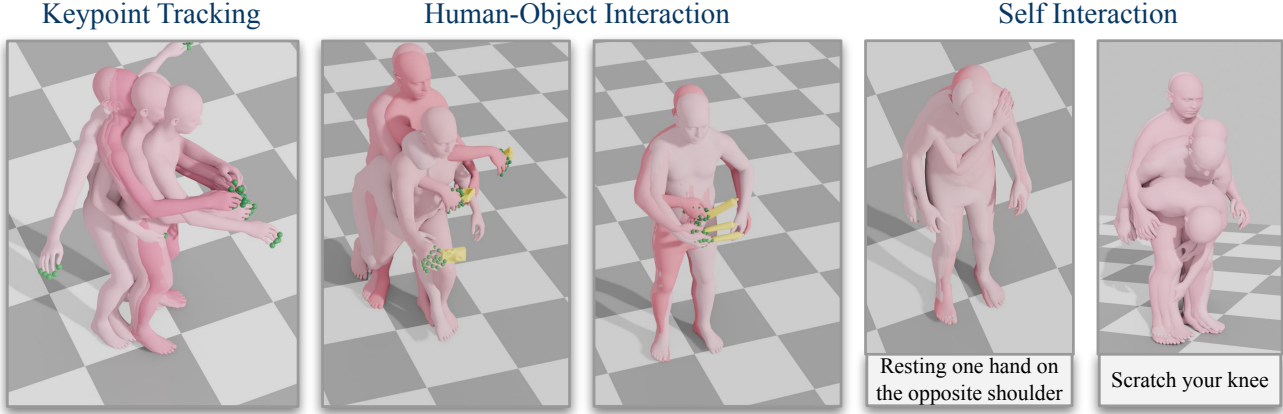


Figure 1. Our method, *FUSION*, enables full-body motion synthesis, including detailed hand motion. Using our optimization framework, we achieve realistic motions for Keypoint Tracking (left), Human–Object Interaction (middle), and Self-Interaction (right) tasks. The initial frames have lighter colors and they get darker over time. To see the motions please watch the supplementary video.

## Abstract

*Hands are central to interacting with our surroundings and conveying gestures, making their inclusion essential for full-body motion synthesis. Despite this, existing human motion synthesis methods fall short: some ignore hand motions entirely, while others generate full-body motions only for narrowly scoped tasks under highly constrained settings. A key obstacle is the lack of large-scale datasets that jointly capture diverse full-body motion with detailed hand articulation. While some datasets capture both, they are limited in scale and diversity. Conversely, large-scale datasets typically focus either on body motion without hands or on hand motions without the body. To overcome this, we curate and unify existing hand motion datasets with large-scale body motion data to generate full-body sequences that capture both hand and body. We then propose the first diffusion-based unconditional full-body motion prior, *FUSION*, which jointly models body and hand motion. Despite using a pose-based motion representation, *FUSION* surpasses State-Of-The-Art (SOTA) skeletal control models on the Keypoint Tracking task in the HumanML3D dataset and achieves superior motion naturalness. Beyond standard benchmarks, we demonstrate that *FUSION* can go beyond typical uses of motion priors*

*through two applications: (1) generating detailed full-body motion including fingers during interaction given the motion of an object, and (2) generating Self-Interaction motions using an Large Language Models (LLM) to transform natural language cues into actionable motion constraints. For these applications, we develop an optimization pipeline that refines the latent space of our diffusion model to generate task-specific motions. Experiments on these tasks highlight precise control over hand motion while maintaining plausible full-body coordination. The code will be public.*

## 1. Introduction

Generating realistic human motion is essential for interactive applications spanning Computer Graphics, Computer Vision, Robotics, and Augmented Reality (AR)/Virtual Reality (VR). A key aspect of realism in these settings is interaction, whether with objects, other people, one’s own body, or the user in a virtual environment. Even a simple act like *drinking water from a glass* combines Human–Object Interaction (HOI) (grasping and manipulating the glass) with Self-Interaction (bringing it to the mouth). This requires coordinated full-body movement: torso leaning, arm and elbow adjustment to avoid collisions, anatomically correct grasps, subtle wrist rotations, and head motion. Any unnatural artifact (e.g. finger penetration) immediately breaks

immersion.

Because such tasks demand different body parts *working in tandem*, it is crucial to capture both body and hand movements within a unified framework. Generating such motions directly from task descriptions or constraints is highly challenging due to the high-dimensional pose space, complex anatomical dependencies, the need for temporal consistency, and the precise coordination required for interactions. To address these challenges, many approaches rely on motion priors, *i.e.* learned models that provide a distribution over plausible human motions, simplifying the task of generating realistic sequences. Yet, most existing models focus solely on body motion, neglecting hand articulation [1–3, 6, 12, 20, 21, 36, 48, 52]. This leads to a disconnect between body and hand behavior, limiting the coherence of motions. While recent methods attempt to address this gap, they remain narrowly scoped [9, 39, 46], targeting specific tasks such as HOI with relatively static body motions and under strong constraints *e.g.* predefined text descriptions, initial body pose, or body motion without hands.

Despite its importance, modeling full-body motions remains largely understudied. A significant barrier is the lack of large-scale datasets that simultaneously capture hand, head, and body motions. While there exist datasets that capture both hand and body, these typically contain very limited body motion [8, 14, 23, 44], making them insufficient for training general-purpose motion priors. In contrast, large-scale datasets capturing rich body motions typically lack detailed hands [21, 26], while others focus narrowly on hand articulation without body motion [4, 27, 28]. As a result, no single dataset offers the scale and diversity of natural full-body motion with hands.

Our key insight is to merge this limited full-body data with large-scale body-only datasets and hand-only datasets. We combine detailed local hand motions with broader body motions to obtain additional full-body sequences. While these augmented sequences are not correlated at the sequence level, they still serve effectively as training data for a motion prior, which models plausible human motions. During downstream motion generation, observation constraints (*e.g.* trajectories, contacts, or task-specific guidance) ensure consistency with the target scenario. We empirically validate this strategy through ablation studies, showing that the joint prior outperforms separate body-only and hand-only priors.

Building on this idea, we propose *FUSION*, a novel unconditional denoising diffusion-based full-body motion prior that jointly models body and hand dynamics. Training an unconditional model is advantageous as it allows leveraging a broad range of motion data without being limited by specific conditioning inputs such as text descriptions, audio signals, or object-related information. By removing these constraints during training, the model learns a more general

and natural representation of human motion. The model can later be adapted or fine-tuned for various targeted applications. To enable such adaptation, we build upon the diffusion noise optimization method DNO [17], extending it to handle flexible constraints from diverse sources, such as keypoint trajectories, high-level instructions from external planners such as LLMs, and object grasping algorithms. This extension broadens the applicability of DNO to unified full-body motion control, capturing both coarse body dynamics and fine-grained finger articulations.

We demonstrate the effectiveness and flexibility of *FUSION* through extensive quantitative and qualitative experiments on Keypoint Tracking, HOI, and Self-Interaction tasks (see Fig. 1, Tab. 1, Fig. 3). In particular, we show that *FUSION* can accurately track spatial trajectories across various body parts. Additionally, given the motion of an object as a constraint, *FUSION* can be used to generate detailed full-body motions that naturally conform to the object’s movement. Lastly, we provide natural language commands (*e.g.*, *touch your head*) to an LLM, which extracts contact-related cues in the form of body vertex constraints over time. *FUSION* then uses these constraints to synthesize Self-Interaction motions that follow given commands.

Overall, our work advances full-body motion synthesis by providing a unified framework that seamlessly integrates coarse motion generation with fine-grained interactive control. In summary, our contributions are as follows:

- We propose a novel way to combine and augment heterogeneous data sources for hands and body, and use them to train *FUSION*, the first unconditional diffusion-based motion prior that synthesizes full-body motions in a unified framework.
- We extend a baseline diffusion noise optimization (DNO) framework with task-specific modifications, enabling our trained motion prior to adapt to diverse downstream applications such as HOI and Self-Interaction.
- We propose a novel pipeline that uses LLMs to convert natural language cues into constraints to generate realistic Self-Interaction motions. Through the optimization we generated a small Self-Interaction dataset that can be useful in other downstream tasks.

## 2. Related Work

### 2.1. Human Motion Synthesis

Motion synthesis methods can be categorized into unconditional and conditional approaches. Unconditional methods generate human motion without control signals. HuMoR [36] uses an autoregressive VAE architecture [19], but this design complicates test-time optimization. NeMF, alleviates this problem through sequential modeling of the human motion [12]. NeMF separates global from local motion with a lightweight representation, performing well in mo-

tion inbetweening and interpolation but is limited in diverse motion synthesis. HMP [7] extends NeMF to hand motions, but it cannot capture coordinated body and hand dynamics, underscoring the need for a unified motion prior.

In contrast, conditional approaches focus on generating motions using specific control inputs. These methods use various conditioning signals such as text descriptions [2, 3, 20, 33, 39, 41, 47, 48, 56], audio [22, 50], trajectories [18, 37], action labels [32], and object-related information [5, 9, 21, 34, 45, 46, 55, 59]. While these approaches enable context-aware motion synthesis, they each require specific data types, limiting the use of available datasets. By contrast, *FUSION* leverages heterogeneous data sources without being bound to specific conditioning signals, while still allowing for flexible control through optimization.

## 2.2. Spatial Control for Human Motion Synthesis

Recent research has focused on controlling motion through spatial cues, particularly joint positions over time. GMD [18] uses a two-stage diffusion approach but controls only 2D pelvis trajectories. OmniControl [54] offers flexible spatial control over various joints using spatial and realism guidance, though it struggles with accurate trajectory alignment. TLCControl [52] achieves better trajectory control through latent code optimization of motion VQ-VAE. However, these methods discard hands and operate in the joint space, requiring post-processing to convert motion into pose space. WANDR [6] addresses this by working directly in pose space and introducing *intention features*, but has no hand articulation and is limited in controlling multiple joints. *FUSION* advances beyond these approaches by providing flexible control over both body and hand motions in a single framework, operating directly in pose space while avoiding the limitations of autoregressive models through our architecture and noise optimization technique.

## 2.3. Controlling Diffusion Models

Diffusion models show strong performance in synthesis tasks but present challenges in control. Existing control methods for diffusion models include classifier guidance [29, 43], classifier-free guidance [13, 16, 38, 40, 57], score distillation [35], and diffusion noise optimization [17, 51]. DNO [17] has successfully applied noise optimization to tasks such as motion inbetweening, dense optimization, keyframe interpolation, and obstacle avoidance. Building on this work, we control our full-body motion model through noise optimization across various tasks. Our approach extends these capabilities by integrating flexible constraints derived from diverse sources ranging from keypoint trajectories to high-level instructions from LLMs or object grasping algorithms. This enables precise control over both coarse body movements and fine-grained finger articulations within a unified framework.

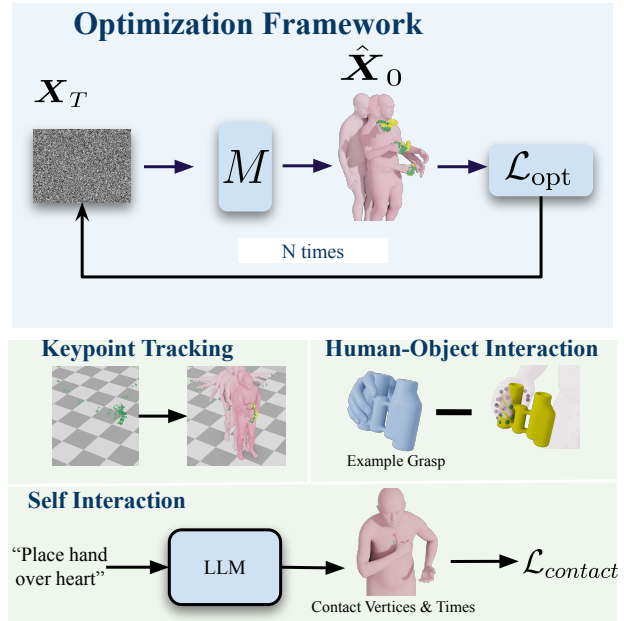


Figure 2. **Method Overview:** Our framework (top) refines diffusion noise through an optimization process that incorporates multiple control signals (middle, bottom). These include example grasps (middle-right), where the difference between human hand joints (pink dots) and grasping hand joints (green dots) guides the optimization. Additionally, joint-based control signals (middle-left picture, green points) serve as loss functions to enforce precise motion constraints. Finally, high-level plans from an LLM (bottom) enable motion synthesis that adheres to specified contact vertices and timesteps, ensuring task-driven and contextually appropriate interactions. For each application our framework leverages backpropagation through the motion denoiser  $M$  to iteratively update the noise. After optimization, the refined noise  $X_T$  is decoded to produce the final motion sequence.

## 3. Method

This section introduces *FUSION*, the first generic motion prior capable of synthesizing full-body motions, describes our novel data fusion strategy that combines heterogeneous hand and body motion datasets, and presents our flexible optimization framework that refines the latent space of our diffusion model using task-specific constraints.

### 3.1. Curating the Dataset

A major limitation in full-body motion synthesis is the scarcity of datasets that include both detailed hand and body motion. Existing datasets that capture both typically focus on HOI or gesture synthesis, where the body remains relatively stable with minimal movement [8, 23, 44]. This limitation has long been a key obstacle to developing a comprehensive motion prior capable of synthesizing realistic hand and body motions together. To overcome this challenge, we employ a method that effectively leverages available data for both hand and body motion.

To obtain body motions, we compile data from AMASS, ARCTIC, OMOMO, SAMP, and BEAT2 [8, 11, 21, 23, 26]. To augment this curated dataset, we apply flipping to both pose and translation, effectively doubling the number of samples while ensuring the motions remain plausible. This straightforward augmentation increases the diversity of body motion sequences without compromising their naturalness. After processing, we have 145,100 sequences, each with 120 timeframes.

For hand motions, we combine data from ARCTIC, TCDHands, GRAB, HOT3D, MOYO, InterHand2.6M, and Re:InterHand [4, 8, 14, 27, 28, 44, 49]. Our augmentation process begins by flipping local left-hand motion sequences to generate right-hand counterparts, while right-hand motions are kept in their original form. This pose-flipping strategy enhances data diversity without compromising motion plausibility. Additionally, we apply time-reversal augmentation by reversing the temporal order of hand motions, which further doubles the dataset while preserving motion realism. From this resulting set of local right-hand motion sequences, we randomly sample segments and integrate them into the full-body motion. For left-hand motions, pose flipping is applied in a post-processing step to ensure consistency. When the body motion is from a full-body dataset that already includes hand motions (e.g., GRAB, ARCTIC, BEAT2, TCDHands), we instead retain the original hand segments to better preserve hand–body dynamics.

In total, we have 41,148 sequences, each with 120 timeframes. Overall, the augmentation strategies improve the model’s ability to generalize to diverse dynamic hand and body motions. Our test split consists of the test sets from the ARCTIC and GRAB datasets [8, 44]. In total, our dataset comprises 17.4M timeframes at 30 FPS, with each sequence containing 120 timeframes. This curated dataset provides a rich resource for full-body motion synthesis.

A key concern when merging body and hand motions is the risk of self-penetration. To address this, we always retain the wrist orientation from the body pose and use only the local hand articulation from the hand motion when merging datasets. Keeping the wrist orientation consistent with the body pose reduces the risk of self-penetration. In addition, we check whether copying local hand motions introduces further self-penetrations and apply penetration-based filtering, discarding physically impossible motions. For dataset ratios and motion merging visualization, we refer readers to Sup.Mat..

### 3.2. Motion Representation

*FUSION* learns 3D human motion by extracting features from SMPL eXpressive (SMPL-X) [31] motion parameters. Recent works on motion editing and synthesis have demonstrated that predicting canonicalized trajectories is advantageous for both synthesis and editing tasks [3, 21, 52, 57].

Building on this observation, we predict the canonicalized trajectory values. A motion sequence  $\mathbf{X} = \{x^1, \dots, x^N\} \in \mathbb{R}^{N \times D}$  consists of a sequence of feature vectors  $x^i \in \mathbb{R}^D$ :

$$x^i := \{\tau^i, \phi^i, \gamma^i, \theta^i, J^i, f^i\}.$$

Here,  $\tau^i \in \mathbb{R}^3$  is the canonicalized root velocity,  $\phi^i \in \mathbb{R}^6$  is the root orientation with respect to the XY plane,  $\gamma^i \in \mathbb{R}^6$  represents the root angular velocity with respect to the Z axis,  $\theta^i \in \mathbb{R}^{324}$  is the local SMPL-X pose in 6D representation [60],  $J^i \in \mathbb{R}^{165}$  is the corresponding joint locations, and  $f^i \in [0, 1]^4$  are the predicted contact probabilities of the foot joints.  $N = 120$  is the sequence length,  $D = 508$  is the feature dimension.

### 3.3. FUSION Formulation

Previous methods have shown the effectiveness of diffusion models for motion generation [3, 21, 41, 48, 54]. Motivated by these results, we train *FUSION* as an unconditional denoising diffusion model with fixed sequence lengths. The model learns the reverse diffusion process of gradually denoising  $X_t$ , starting from pure Gaussian noise  $X_T$ :  $P_{\theta_M}(X_{t-1} | X_t) = \mathcal{N}(\mu_t(\theta_M), (1 - \alpha_t) \mathbf{I})$ , where  $\theta_M$  is the denoising diffusion model parameters,  $X_t \in \mathbb{R}^{N \times D}$  represents the motion state at the  $t^{\text{th}}$  step of the noising process, and  $T = 300$  denotes the total number of denoising steps. The hyperparameters  $\alpha_t \in (0, 1)$  progressively decrease to 0 as  $t \rightarrow T$ . Inspired by [48], our model directly estimates the final clean motion  $\hat{X}_0(\theta_M) := M(X_t, t; \theta_M)$ , where  $M$  is the motion denoiser model. The model is trained through the reconstruction, geometry, and foot skating losses:

$$\begin{aligned} \mathcal{L}_{\text{recon}} &:= E_{t \sim \text{DiscreteUniform}[1, T]} \|X_0 - \hat{X}_0\|_2^2, \\ \mathcal{L}_{\text{geo}} &:= \frac{1}{N} \sum_{i=1}^N \|FK(x_0^i) - FK(\hat{x}_0^i)\|_2^2, \\ \mathcal{L}_{\text{foot}} &:= \frac{1}{N-1} \sum_{i=1}^{N-1} \|(FK(\hat{x}_0^{i+1}) - FK(\hat{x}_0^i)) \cdot f^i\|_2^2, \end{aligned} \quad (1)$$

where  $X_0$  denotes the Ground Truth (GT) motion sequence,  $FK(\cdot)$  denotes the forward kinematics function of the SMPL-X body model [31],  $x_0^i$  is the GT pose sample,  $\hat{x}_0^i$  is the denoised pose sample, and  $f^i \in \{0, 1\}$  is the binary contact prediction at frame  $i$ . The term  $\mathcal{L}_{\text{geo}}$  ensures that the predicted joints are close to those computed via forward kinematics, and  $\mathcal{L}_{\text{foot}}$  mitigates foot skating.

### 3.4. FUSION Implementation details

We base our model on MotionFix [3] and modify its transformer encoder architecture. The architecture consists of 19.7M trainable parameters. The learning rate is set to  $10^{-4}$ , and the batch size is 32, with a total of 300,000 training steps. We use the AdamW [25] optimizer. The forward

diffusion step count  $T$  is set to 300. The loss hyperparameters are  $\lambda_{\text{recon}} = 1$ ,  $\lambda_{\text{geo}} = 1$ , and  $\lambda_{\text{foot}} = 1$ . For more implementation details, please refer to the project webpage.

### 3.5. Diffusion Noise Optimization

Unconditional motion priors allow the model to learn a diverse latent space without requiring labeled or task-specific training data. However, without conditioning or constraints, they are not directly useful for specific downstream tasks such as HOI, Self-Interaction, or other forms of motion that depend on external conditions (see Sec. 4). To make them practical, it is essential to control the generated motion so that it aligns with task-specific requirements. This calls for a framework to control the motion. Recently, DNO [17] has demonstrated that optimizing diffusion noise is an effective way to perform motion synthesis for various tasks.

DNO [17] treats the diffusion noise  $x_T \sim \mathcal{N}(0, I)$  as the latent variable and generates motion with the full sampling process of the trained diffusion model  $M$ , resolved using the ODE formulation of DDIM [42]. The optimization is then defined over  $x_T$ , with gradients propagating through all denoising steps:

$$x_T^* := \arg \min_{x_T} \{ \mathcal{L}_{\text{opt}}(\text{ODE}(M, x_T)) + \mathcal{L}_{\text{decorr}}(x_T) \}$$

where the final output will be  $x^* = \text{ODE}(M, x_T^*)$ . Here,  $\mathcal{L}_{\text{decorr}}$  is a decorrelation regularizer [15] that encourages  $x_T$  to remain within the Gaussian prior.  $\mathcal{L}_{\text{opt}}$  includes several loss terms to guide the motion towards both realism and task compliance:

$$\mathcal{L}_{\text{opt}} := \lambda_{\text{lk}} \mathcal{L}_{\text{lk}} + \lambda_{\text{foot}} \mathcal{L}_{\text{foot}} + \lambda_{\text{ch}} \mathcal{L}_{\text{ch}} + \lambda_{\text{close}} \mathcal{L}_{\text{close}}, \quad (2)$$

where  $\mathcal{L}_{\text{lk}}$  encourages the diffusion noise to remain close to zero (the prior mean),  $\mathcal{L}_{\text{ch}}$  penalizes foot deviation from ground when in contact, and  $\mathcal{L}_{\text{close}}$  enforces tracking of specified keypoints over time. Specifically, let  $c_j^k \in \mathbb{R}^3$  denote the target location for the joint (or vertex)  $j$  at the keyframe  $k$ , and let  $\hat{c}_j^k$  be its computed location from the denoised motion  $\hat{x}_0$ . We then define:

$$\begin{aligned} \mathcal{L}_{\text{lk}} &:= \frac{1}{N} \sum_{i=1}^N \|x_T^i\|_2^2, \\ \mathcal{L}_{\text{ch}} &:= \frac{1}{N-1} \sum_{i=1}^{N-1} \|FK(\hat{x}_0^i)_z \cdot f^i\|_1, \\ \mathcal{L}_{\text{close}}(\mathbf{x}, O) &:= \frac{1}{|O|} \sum_{(j,k) \in O} \|\hat{c}_j^k(\hat{x}_0) - c_j^k\|_1, \end{aligned} \quad (3)$$

Here,  $O$  denotes the observed set containing  $(j, k)$  pairs corresponding to target joints and keyframes determined by the task.  $\mathcal{L}_{\text{opt}}$  can include other types of losses, such as penetration loss or contact loss, depending on the specific application. Fig. 2 shows an overview of our optimization setup

and different constraints from downstream tasks. For hyperparameter values for the optimization, we refer to Sup.Mat..

## 4. Applications

*FUSION* unlocks a broad range of applications by providing a unified motion prior that synthesizes full-body and finger motions. By combining body and finger articulation, our method captures fine-grained interactions, and using our diffusion noise optimization framework, it can be efficiently guided when provided with task-specific requirements. In the following sections, we demonstrate how this capability allows our method to handle diverse scenarios ranging from HOI to Self-Interaction planning via language cues.

### 4.1. Human–Object Interaction

A primary application of our method lies in HOI. By synthesizing both body and hand (including finger) motions, our framework enables realistic grasping and manipulation. To demonstrate this, we generate stable grasps by employing GRABNet [44], a static grasp synthesis method that generates hand poses conditioned on the object geometry. GRABNet provides a static grasp configuration for a given object, which we assume remains stable throughout the object’s motion. Under this assumption, we optimize the hand joint trajectories using a closeness loss  $\mathcal{L}_{\text{close}}$ . This generates realistic full-body motions that interact with objects while having natural finger articulation before grasping the object. Fig. 3 illustrates sample results, and additional visualizations are provided in the supplementary video. Our optimization framework is designed in a plug-and-play fashion, which allows seamless integration with various constraints. This flexibility enables our system to adapt to different object shapes and interaction scenarios, thereby facilitating diverse applications in Robotics and AR/VR.

### 4.2. Self-Interaction using LLMs

Our method can also be extended to scenarios involving Self-Interaction, where high-level semantic guidance is required. For this purpose we leverage recent advances in LLMs through a novel pipeline that generates structured contact plans. For this, we sample 236 vertices on the human body, each with a semantic label that may be important for the Self-Interaction task. These points, along with their semantic labels, are included in a textual prompt that also contains curated samples and explanations for meaningful interaction predictions. This prompt is given to an instance of GPT-3 without any fine-tuning [30]. The model predicts which parts should be in contact and at what timestamps, based on a high-level action description. For instance, given prompts such as *clap your hands*, the LLM outputs a set  $\nu = \{(j^{\tau_1}, k^{\tau_1}, \tau_1), (j^{\tau_2}, k^{\tau_2}, \tau_2), \dots\}$  indicating the targeted vertices  $j^{\tau_i}, k^{\tau_i}$  and corresponding timestamps  $\tau_i$ . This information takes into account the dynamics

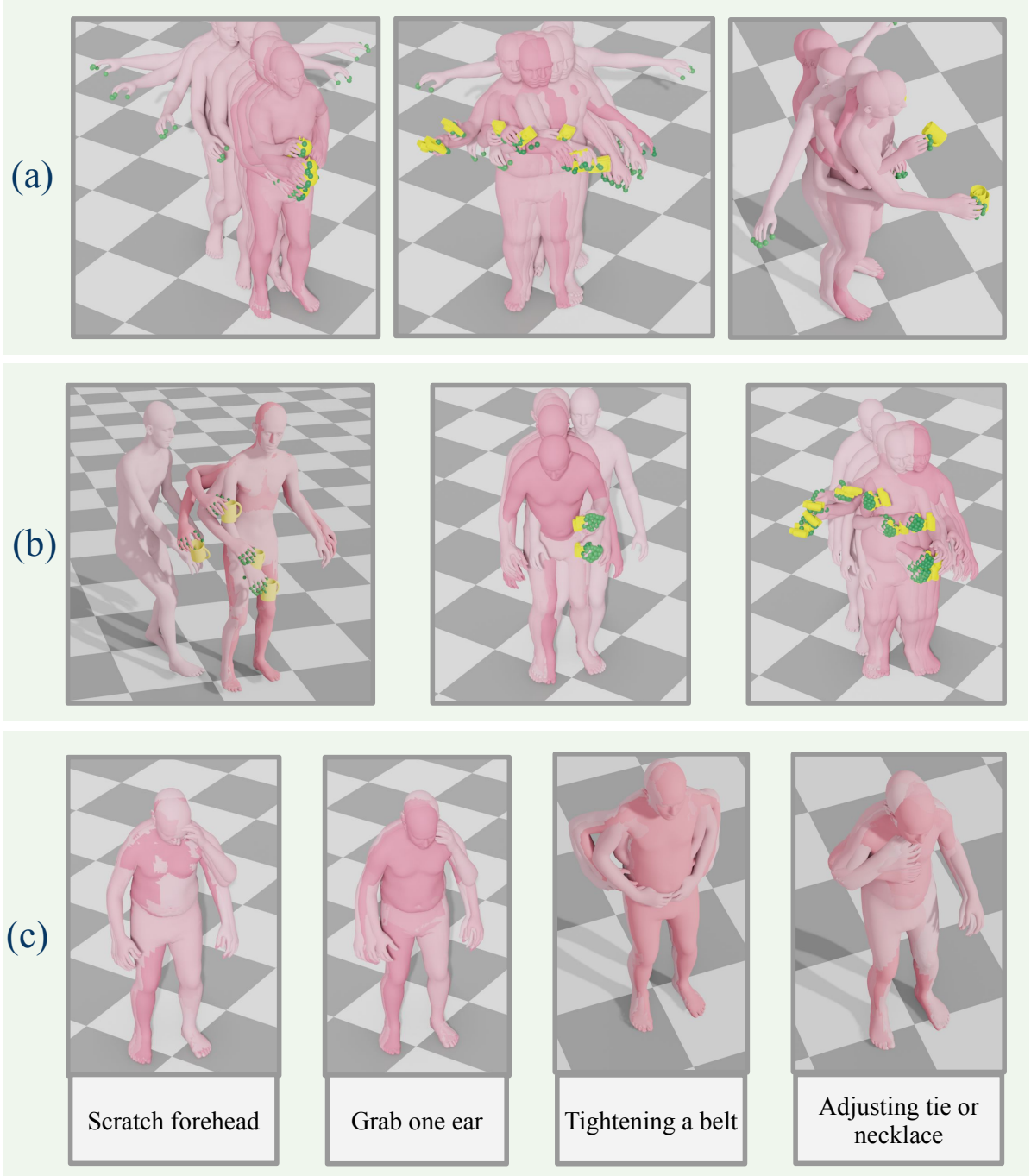


Figure 3. **FUSION qualitative results:** *FUSION* can track any given joint location (all 10 fingertips) over time (a). Conform a grasp provided by an off-the-shelf method (b) or Self-Interaction (c). In this case, it tracks the fingertips. Objects are provided only for visualization purposes, they do not play any role in the input. Mesh colors darken over time.

of the motion as it includes timestamps and is then enforced via a contact loss, defined as:

$$\mathcal{L}_{\text{contact}}(\mathbf{x}, \nu) := \frac{1}{|\nu|} \sum_{(j^\tau, k^\tau, \tau) \in \nu} \|\hat{\mathbf{v}}_{j^\tau}(\mathbf{x}) - \hat{\mathbf{v}}_{k^\tau}(\mathbf{x})\|_1.$$

Here  $\hat{\mathbf{v}}_{j^\tau}(\mathbf{x})$  indicates vertex location with index  $j^\tau$ . This loss ensures that the specified body parts are in contact at the desired times, enabling structured and interpretable motion planning. Fig. 3 shows the qualitative examples of self-contact guided by LLM outputs. For sampled points on the body and further qualitative examples, we refer to Sup.Mat..

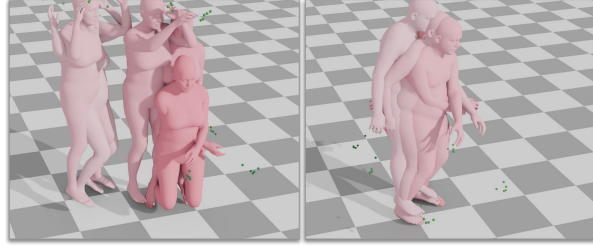


Figure 4. **FUSION failure cases.** When the trajectory is highly dynamic, *FUSION* may fail to comply with task-specific requirements, which can lead to self-penetration and unrealistic motion. The example above illustrates this for the Keypoint Tracking task.

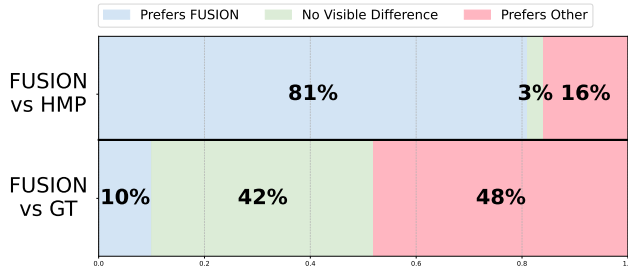


Figure 5. **Subject preference ratios on test split.** Subjects were tasked with selecting one of three options: preferring *FUSION*, reporting no visible difference, and preferring the other method.

**Failure Cases:** *FUSION* fails in highly dynamic scenarios (Fig. 4), leading to self-penetration and unnatural motion.

## 5. Experiments

We provide experimental evaluations to test the performance of *FUSION*. We compare our approach with SOTA motion generation models on Keypoint Tracking performance and motion realism and perform ablation studies to assess design choices on motion synthesis quality.

### 5.1. Comparison with SOTA methods

We compare *FUSION* with previous SOTA motion generation models: MDM, PriorMDM, GMD, OmniControl, and TLCControl [18, 41, 48, 52, 54], on the Keypoint Tracking task using the HumanML3D dataset [10]. We evaluate tracking performance on six key joints: Pelvis, Head, Left Wrist, Right Wrist, Left Foot, and Right Foot, using Trajectory Error, Location Error, and Average Error as per previous methods [48, 52, 54]. Notably, *FUSION* is unconditional and operates directly on a pose-based representation of the SMPL-X body model [31] instead of a skeletal representation of the SMPL model [24]. As such, unlike the other baselines, we cannot compute FID, KID, Diversity, and R-Precision metrics. Tab. 1 provides an overview of the performance on the HumanML3D dataset [10]. This comparison demonstrates that our approach achieves competitive performance in terms of control accuracy and outperforms in motion realism (Sec. 5.2). However, where our perfor-

mance lags, it can be attributed to the trade-off between expressiveness and metric-specific evaluations that favor rigid skeletal representations.

### 5.2. Qualitative Comparison

Keypoint Tracking should be performed without compromising motion realism to preserve naturalness. Since all previous Keypoint Tracking methods operate on the SMPL body model, for a fair comparison, we evaluate the synthesized body and hand motions separately.

For comparing the realism of the synthesized body motions, we use a SOTA method for motion evaluation: MotionCritic [53]. Given a body motion in SMPL pose format, MotionCritic evaluates the realism and outputs a numerical score. To ensure compatibility, we only use the body pose generated by *FUSION* (local hand motions excluded), with wrist orientations set to the identity rotation. As Tab. 1 shows, compared to the previous SOTA joint tracking method TLCControl [52], *FUSION* outperforms it on the motion realism metric. For hand motion synthesis, we conduct a perceptual study comparing *FUSION* with both the GT and HMP [7] on the Keypoint Tracking task, which involves tracking all 10 fingertips on our test split. Participants were asked to evaluate the realism of motions involving the interaction of both hands with objects. Fig. 5 shows the subject preference ratios. The results indicate that *FUSION* synthesizes more realistic hand motions than HMP and achieves a level of realism comparable to the GT. For more details, we refer to Sup.Mat..

### 5.3. Quantitative Analysis of LLM

Since high-level instructions for Self-Interaction are taken from an LLM, the quality of the synthesized motions depends on the quality of the high-level planning. To assess the reliability of the planning, we use a second instance of GPT-o3 [30] to perform the reverse reasoning, *i.e.*, prompting it with only 4 output samples of the first instance of GPT-o3 to get the instruction that describes the motion. Then, we compare the initial instructions with those obtained from the second model using BERTScore, focusing on the F1 metric, which provides a measure of semantic similarity [58]. Tab. 3 presents two representative sentence pairs with the highest and lowest F1 scores, illustrating the quality of alignment. These examples suggest that the model can successfully infer semantically aligned instructions from its outputs. For the details, we refer to Sup.Mat..

### 5.4. Ablation Studies

**Unified Motion Prior Optimization:** To assess the benefits of a unified representation that jointly models hand and body motion, we conduct an ablation study comparing our method with a sequential optimization approach. In the sequential variant, the model is first optimized for hand mo-

Method	Control Joint	Traj. Error ↓ (50 cm, %)	Traj. Error ↓ (10 cm, %)	Traj. Error ↓ (5 cm, %)	Loc. Error ↓ (50 cm, %)	Loc. Error ↓ (10 cm, %)	Loc. Error ↓ (5 cm, %)	Avg. Error ↓ (cm)	Motion Realism ↑ [53]
MDM PriorMDM GMD OmniControl TLControl <b>Ours</b>	Pelvis	40.22	-	-	30.76	-	-	59.59	-
		34.57	-	-	21.32	-	-	44.17	-
		9.31	-	-	3.21	-	-	14.39	-
		3.87	-	-	0.96	-	-	3.38	-
		<b>0.00</b>	<b>0.39</b>	<b>11.04</b>	<b>0.00</b>	<b>0.00</b>	<b>0.26</b>	<b>1.08</b>	-3.89
		<b>0.00</b>	1.47	12.41	<b>0.00</b>	0.13	0.68	1.16	<b>0.37</b>
OmniControl TLControl <b>Ours</b>	Head	4.22	-	-	0.79	-	-	3.49	-
		<b>0.00</b>	<b>1.10</b>	22.95	<b>0.00</b>	<b>0.07</b>	0.89	<b>1.10</b>	-7.47
		<b>0.00</b>	2.03	<b>13.24</b>	<b>0.00</b>	0.15	<b>0.44</b>	1.51	<b>-0.32</b>
OmniControl TLControl <b>Ours</b>	Left Wrist	8.01	-	-	1.34	-	-	5.29	-
		<b>0.00</b>	<b>1.37</b>	12.88	<b>0.00</b>	<b>0.11</b>	<b>0.28</b>	<b>1.08</b>	-5.66
		<b>0.00</b>	2.93	<b>5.54</b>	<b>0.00</b>	0.13	0.35	1.23	<b>-0.79</b>
OmniControl TLControl <b>Ours</b>	Right Wrist	8.13	-	-	1.27	-	-	5.19	-
		<b>0.00</b>	<b>1.17</b>	12.30	<b>0.00</b>	<b>0.02</b>	<b>0.18</b>	<b>1.09</b>	-5.62
		<b>0.00</b>	3.03	<b>6.57</b>	<b>0.00</b>	0.15	0.38	1.31	<b>-0.83</b>
OmniControl TLControl <b>Ours</b>	Left Foot	5.94	-	-	0.94	-	-	3.14	-
		<b>0.00</b>	<b>0.00</b>	<b>10.12</b>	<b>0.00</b>	<b>0.01</b>	<b>0.15</b>	<b>1.14</b>	-4.79
		<b>0.00</b>	3.62	13.04	<b>0.00</b>	0.54	0.87	1.42	<b>-1.13</b>
OmniControl TLControl <b>Ours</b>	Right Foot	6.66	-	-	1.20	-	-	3.34	-
		<b>0.00</b>	<b>0.49</b>	<b>11.13</b>	<b>0.00</b>	<b>0.00</b>	<b>0.16</b>	<b>1.16</b>	-3.15
		<b>0.00</b>	2.75	12.82	<b>0.00</b>	0.24	0.74	1.46	<b>-0.72</b>
OmniControl TLControl <b>Ours</b>	All Joints above	75.59	-	-	12.30	-	-	23.67	-
		<b>0.00</b>	<b>10.62</b>	71.09	<b>0.00</b>	<b>0.09</b>	<b>1.71</b>	<b>1.57</b>	-7.86
		<b>0.00</b>	35.28	<b>64.14</b>	<b>0.00</b>	1.05	3.73	1.78	<b>-1.26</b>

Table 1. Quantitative comparison with previous SOTA methods. The best scores are highlighted bold for Keypoint Tracking on HumanML3D. Although *FUSION* controls pose rather than spatial joint locations, it performs on par with SOTA skeletal control methods. On motion realism our method outperforms previous SOTA method TLControl [52] and reports close numbers to the ground truth.

Method	Control Joint	Skating ratio (%) ↓	Loc. Err. ↓ (30 cm, %)	Loc. Err. ↓ (10 cm, %)	Loc. Err. ↓ (5 cm, %)	Avg. Err. (cm) ↓
<i>FUSION</i>	Finger Tips	<b>6.03</b>	<b>0.00</b>	<b>0.03</b>	<b>0.29</b>	<b>0.59</b>
Sequential <i>FUSION</i>	Finger Tips + Wrists	13.80	<b>0.00</b>	0.25	2.19	1.23
HMP [7] + TLControl [52]	Finger Tips + Wrists	15.35	<b>0.00</b>	0.32	4.02	1.64

Table 2. Ablation studies on the test split. Results emphasize the advantage of having a compact method over optimizing two separate priors. In addition, *FUSION* outperforms the combination of SOTA hand and body motion models in Keypoint Tracking.

Instruction	Predicted Sentence	R	P	F1
Stay in attention position	Stand with both palms on your back thighs, heels pressed together.	0.804	0.830	0.817
Put your hands on your hips	Place your hands on your hips.	0.981	0.977	0.979
Average values		0.894	0.9	0.897

Table 3. Examples of instruction–LLM prediction pairs for the highest, lowest, and average BERTScore F1 values.

tion (given 10 fingertip trajectories) and subsequently for body motion (given wrist trajectories from optimized hand motions). Results are shown in Tab. 2. The first row refers to our baseline method. The second row stands for the sequential variant of our method. Our experiments indicate that the sequential approach leads to increased foot skating and higher trajectory errors. In contrast, optimizing the unified motion prior not only improves performance but also offers superior computational efficiency. To ensure a fair comparison, all experiments used identical learning rates, loss functions, and epoch counts. We refer to Sup.Mat..

**Comparison with combined off-the-shelf priors:** Since to the best of our knowledge, no previous motion-prior includes both body and hands in a unified model, we evaluate our method against a combined model that integrates SOTA hand and body motion priors (HMP and TLControl, respectively) [7, 52]. In this baseline, hand motion is first opti-

mized, and the resulting wrist trajectories are used to subsequently optimize the body motion. We report the results in the last row of Tab. 2 and show that *FUSION* outperforms this two-stage process in overall tracking quality metrics.

## 6. Conclusion

In this work, we present *FUSION*, the first unconditional full-body motion prior on SMPL-X, jointly modeling both body and articulated hand motions. Unlike existing approaches that treat hands and body separately, our method integrates heterogeneous datasets and leverages a denoising diffusion model to capture fine-grained motion dynamics across the entire body. We further adapt a flexible optimization framework that refines the latent diffusion noise under task-specific constraints. Experiments show that *FUSION* achieves competitive performance with the skeleton-based SOTA method in Keypoint Tracking and surpasses it in terms of motion realism. Beyond conventional uses of motion priors, *FUSION* enables applications such as HOI and Self-Interaction. Overall, *FUSION* provides a promising data-driven solution for realistic full-body motion synthesis in fields such as Computer Vision, Robotics, and AR/VR.

## References

[1] Nikos Athanasiou, Mathis Petrovich, Michael J. Black, and G  l Varol. Teach: Temporal action compositions for 3d humans. In *International Conference on 3D Vision (3DV)*, 2022. 2

[2] Nikos Athanasiou, Mathis Petrovich, Michael J. Black, and G  l Varol. SINC: Spatial composition of 3D human motions for simultaneous action generation. *ICCV*, 2023. 3

[3] Nikos Athanasiou, Alp  r Ceske, Markos Diomataris, Michael J. Black, and G  l Varol. MotionFix: Text-driven 3d human motion editing. In *SIGGRAPH Asia 2024 Conference Papers*, 2024. 2, 3, 4

[4] Prithviraj Banerjee, Sindi Shkodrani, Pierre Moulon, Shreyas Hampali, Shangchen Han, Fan Zhang, Linguang Zhang, Jade Fountain, Edward Miller, Selen Basol, Richard Newcombe, Robert Wang, Jakob Julian Engel, and Tomas Hodan. HOT3D: Hand and object tracking in 3D from egocentric multi-view videos. *CVPR*, 2025. 2, 4

[5] Sammy Christen, Shreyas Hampali, Fadime Sener, Edoardo Remelli, Tomas Hodan, Eric Sauser, Shugao Ma, and Bugra Tekin. Diffh2o: Diffusion-based synthesis of hand-object interactions from textual descriptions. In *SIGGRAPH Asia 2024 Conference Papers*, 2024. 3

[6] Markos Diomataris, Nikos Athanasiou, Omid Taheri, Xi Wang, Otmar Hilliges, and Michael J. Black. WANDR: Intention-guided human motion generation. In *Proceedings IEEE Conference on Computer Vision and Pattern Recognition (CVPR)*, 2024. 2, 3

[7] Enes Duran, Muhammed Kocabas, Vasileios Choutas, Zicong Fan, and Michael J. Black. Hmp: Hand motion priors for pose and shape estimation from video. In *Proceedings of the IEEE/CVF Winter Conference on Applications of Computer Vision (WACV)*, pages 6353–6363, 2024. 3, 7, 8, 1

[8] Zicong Fan, Omid Taheri, Dimitrios Tzionas, Muhammed Kocabas, Manuel Kaufmann, Michael J. Black, and Otmar Hilliges. ARCTIC: A dataset for dexterous bimanual hand-object manipulation. In *Proceedings IEEE Conference on Computer Vision and Pattern Recognition (CVPR)*, 2023. 2, 3, 4

[9] Anindita Ghosh, Rishabh Dabral, Vladislav Golyanik, Christian Theobalt, and Philipp Slusallek. Imos: Intent-driven full-body motion synthesis for human-object interactions. In *Eurographics*, 2023. 2, 3

[10] Chuan Guo, Shihao Zou, Xinxin Zuo, Sen Wang, Wei Ji, Xingyu Li, and Li Cheng. Generating diverse and natural 3d human motions from text. In *Proceedings of the IEEE/CVF Conference on Computer Vision and Pattern Recognition (CVPR)*, pages 5152–5161, 2022. 7

[11] Mohamed Hassan, Duygu Ceylan, Ruben Villegas, Jun Saito, Jimei Yang, Yi Zhou, and Michael Black. Stochastic scene-aware motion prediction. In *Proceedings of the International Conference on Computer Vision 2021*, 2021. 4

[12] Chengan He, Jun Saito, James Zachary, Holly Rushmeier, and Yi Zhou. Nemf: Neural motion fields for kinematic animation. In *NeurIPS*, 2022. 2

[13] Jonathan Ho and Tim Salimans. Classifier-free diffusion guidance. In *NeurIPS 2021 Workshop on Deep Generative Models and Downstream Applications*, 2021. 3

[14] Ludovic Hoyet, Kenneth Ryall, Rachel McDonnell, and Carol O’Sullivan. Sleight of hand: Perception of finger motion from reduced marker sets. In *Proceedings of the ACM SIGGRAPH Symposium on Interactive 3D Graphics and Games*, pages 79–86, 2012. 2, 4

[15] Tero Karras, Samuli Laine, Miika Aittala, Janne Hellsten, Jaakko Lehtinen, and Timo Aila. Analyzing and improving the image quality of stylegan. In *2020 IEEE/CVF Conference on Computer Vision and Pattern Recognition (CVPR)*, pages 8107–8116, 2020. 5

[16] Tero Karras, Miika Aittala, Tuomas Kynk  nniemi, Jaakko Lehtinen, Timo Aila, and Samuli Laine. Guiding a diffusion model with a bad version of itself. In *The Thirty-eighth Annual Conference on Neural Information Processing Systems*, 2024. 3

[17] Korrawe Karunratanakul, Konpat Preechakul, Emre Aksan, Thabo Beeler, Supasorn Suwajanakorn, and Siyu Tang. Optimizing diffusion noise can serve as universal motion priors. *2024 IEEE/CVF Conference on Computer Vision and Pattern Recognition (CVPR)*, pages 1334–1345, 2023. 2, 3, 5

[18] Korrawe Karunratanakul, Konpat Preechakul, Supasorn Suwajanakorn, and Siyu Tang. Guided motion diffusion for controllable human motion synthesis. *2023 IEEE/CVF International Conference on Computer Vision (ICCV)*, pages 2151–2162, 2023. 3, 7

[19] Diederik P. Kingma and Max Welling. Auto-encoding variational bayes. In *ICLR*, 2014. 2

[20] Chuqiao Li, Julian Chibane, Yannan He, Naama Pearl, Andreas Geiger, and Gerard Pons-Moll. Unimotion: Unifying 3d human motion synthesis and understanding. *arXiv preprint arXiv:2409.15904*, 2024. 2, 3

[21] Jiaman Li, Jiajun Wu, and C Karen Liu. Object motion guided human motion synthesis. *ACM Trans. Graph.*, 42(6), 2023. 2, 3, 4

[22] Ruilong Li, Sha Yang, David A. Ross, and Angjoo Kanazawa. Ai choreographer: Music conditioned 3d dance generation with aist++. *2021 IEEE/CVF International Conference on Computer Vision (ICCV)*, pages 13381–13392, 2021. 3

[23] Haiyang Liu, Zihao Zhu, Giorgio Becherini, Yichen Peng, Mingyang Su, You Zhou, Xuefei Zhe, Naoya Iwamoto, Bo Zheng, and Michael J. Black. EMAGE: Towards unified holistic co-speech gesture generation via expressive masked audio gesture modeling. In *IEEE/CVF Conf. on Computer Vision and Pattern Recognition (CVPR)*, 2024. 2, 3, 4

[24] Matthew Loper, Naureen Mahmood, Javier Romero, Gerard Pons-Moll, and Michael J. Black. SMPL: A skinned multi-person linear model. *ACM Trans. Graphics (Proc. SIGGRAPH Asia)*, 34(6):248:1–248:16, 2015. 7

[25] Ilya Loshchilov and Frank Hutter. Decoupled weight decay regularization. In *International Conference on Learning Representations*, 2017. 4

[26] Naureen Mahmood, Nima Ghorbani, Nikolaus F. Troje, Gerard Pons-Moll, and Michael J. Black. AMASS: Archive of motion capture as surface shapes. In *International Conference on Computer Vision*, pages 5442–5451, 2019. 2, 4

[27] Gyeongsik Moon, Shoou-I Yu, He Wen, Takaaki Shiratori, and Kyoung Mu Lee. Interhand2.6m: A dataset and baseline for 3d interacting hand pose estimation from a single rgb image. In *European Conference on Computer Vision (ECCV)*, 2020. 2, 4

[28] Gyeongsik Moon, Shunsuke Saito, Weipeng Xu, Rohan Joshi, Julia Buffalini, Harley Bellan, Nicholas Rosen, Jesse Richardson, Mize Mallorie, Philippe Bree, Tomas Simon, Bo Peng, Shubham Garg, Kevyn McPhail, and Takaaki Shiratori. A dataset of relighted 3D interacting hands. In *NeurIPS Track on Datasets and Benchmarks*, 2023. 2, 4

[29] Alex Nichol and Prafulla Dhariwal. Improved denoising diffusion probabilistic models. *ArXiv*, abs/2102.09672, 2021. 3

[30] OpenAI. Introducing o3 and o4-mini, 2024. Accessed: 2025-05-16. 5, 7, 1

[31] Georgios Pavlakos, Vasileios Choutas, Nima Ghorbani, Timo Bolkart, Ahmed A. A. Osman, Dimitrios Tzionas, and Michael J. Black. Expressive body capture: 3D hands, face, and body from a single image. In *Proceedings IEEE Conf. on Computer Vision and Pattern Recognition (CVPR)*, pages 10975–10985, 2019. 4, 7

[32] Mathis Petrovich, Michael J. Black, and Güл Varol. Action-conditioned 3D human motion synthesis with transformer VAE. In *Proc. International Conference on Computer Vision (ICCV)*, pages 10965–10975, Piscataway, NJ, 2021. IEEE. 3

[33] Mathis Petrovich, Michael J. Black, and Güл Varol. TMR: Text-to-motion retrieval using contrastive 3D human motion synthesis. In *International Conference on Computer Vision (ICCV)*, 2023. 3

[34] Huaijin Pi, Sida Peng, Minghui Yang, Xiaowei Zhou, and Hujun Bao. Hierarchical generation of human-object interactions with diffusion probabilistic models. In *Proceedings of the IEEE/CVF International Conference on Computer Vision (ICCV)*, pages 15061–15073, 2023. 3

[35] Ben Poole, Ajay Jain, Jonathan T. Barron, and Ben Mildenhall. Dreamfusion: Text-to-3d using 2d diffusion. *arXiv*, 2022. 3

[36] Davis Rempe, Tolga Birdal, Aaron Hertzmann, Jimei Yang, Srinath Sridhar, and Leonidas J. Guibas. Humor: 3d human motion model for robust pose estimation. In *International Conference on Computer Vision (ICCV)*, 2021. 2

[37] Davis Rempe, Zhengyi Luo, Xue Bin Peng, Ye Yuan, Kris Kitani, Karsten Kreis, Sanja Fidler, and Or Litany. Trace and pace: Controllable pedestrian animation via guided trajectory diffusion. In *Conference on Computer Vision and Pattern Recognition (CVPR)*, 2023. 3

[38] Robin Rombach, A. Blattmann, Dominik Lorenz, Patrick Esser, and Björn Ommer. High-resolution image synthesis with latent diffusion models. *2022 IEEE/CVF Conference on Computer Vision and Pattern Recognition (CVPR)*, pages 10674–10685, 2021. 3

[39] Roey Ron, Guy Tevet, Haim Sawdayee, and Amit H. Bermano. Hoidini: Human-object interaction through diffusion noise optimization, 2025. 2, 3

[40] Chitwan Saharia, William Chan, Saurabh Saxena, Lala Lit, Jay Whang, Emily Denton, Seyed Kamyar Seyed Ghasemipour, Burcu Karagol Ayan, S. Sara Mahdavi, Raphael Gontijo-Lopes, Tim Salimans, Jonathan Ho, David J Fleet, and Mohammad Norouzi. Photorealistic text-to-image diffusion models with deep language understanding. In *Proceedings of the 36th International Conference on Neural Information Processing Systems*, Red Hook, NY, USA, 2022. Curran Associates Inc. 3

[41] Yoni Shafir, Guy Tevet, Roy Kapon, and Amit Haim Bermano. Human motion diffusion as a generative prior. In *The Twelfth International Conference on Learning Representations*, 2024. 3, 4, 7

[42] Jiaming Song, Chenlin Meng, and Stefano Ermon. Denoising diffusion implicit models. In *International Conference on Learning Representations*, 2021. 5

[43] Yang Song, Jascha Sohl-Dickstein, Diederik P Kingma, Abhishek Kumar, Stefano Ermon, and Ben Poole. Score-based generative modeling through stochastic differential equations. In *International Conference on Learning Representations*, 2021. 3

[44] Omid Taheri, Nima Ghorbani, Michael J. Black, and Dimitrios Tzionas. GRAB: A dataset of whole-body human grasping of objects. In *European Conference on Computer Vision (ECCV)*, 2020. 2, 3, 4, 5

[45] Omid Taheri, Vasileios Choutas, Michael J. Black, and Dimitrios Tzionas. GOAL: Generating 4D whole-body motion for hand-object grasping. In *Conference on Computer Vision and Pattern Recognition (CVPR)*, 2022. 3

[46] Omid Taheri, Yi Zhou, Dimitrios Tzionas, Yang Zhou, Duygu Ceylan, Soren Pirk, and Michael J. Black. GRIP: Generating interaction poses using latent consistency and spatial cues. In *International Conference on 3D Vision (3DV)*, 2024. 2, 3

[47] Guy Tevet, Brian Gordon, Amir Hertz, Amit H Bermano, and Daniel Cohen-Or. Motionclip: Exposing human motion generation to clip space. In *Computer Vision–ECCV 2022: 17th European Conference, Tel Aviv, Israel, October 23–27, 2022, Proceedings, Part XXII*, pages 358–374. Springer, 2022. 3

[48] Guy Tevet, Sigal Raab, Brian Gordon, Yoni Shafir, Daniel Cohen-or, and Amit Haim Bermano. Human motion diffusion model. In *The Eleventh International Conference on Learning Representations*, 2023. 2, 3, 4, 7

[49] Shashank Tripathi, Lea Müller, Chun-Hao P. Huang, Taheri Omid, Michael J. Black, and Dimitrios Tzionas. 3D human pose estimation via intuitive physics. In *Conference on Computer Vision and Pattern Recognition (CVPR)*, pages 4713–4725, 2023. 4

[50] Jonathan Tseng, Rodrigo Castellon, and C Karen Liu. Edge: Editable dance generation from music. *arXiv preprint arXiv:2211.10658*, 2022. 3

[51] Bram Wallace, Akash Gokul, Stefano Ermon, and Nikhil Naik. End-to-End Diffusion Latent Optimization Improves Classifier Guidance. In *2023 IEEE/CVF International Conference on Computer Vision (ICCV)*, pages 7246–7256, Los Alamitos, CA, USA, 2023. IEEE Computer Society. 3

[52] Weilin Wan, Zhiyang Dou, Taku Komura, Wenping Wang, Dinesh Jayaraman, and Lingjie Liu. Tlcontrol: Trajectory

and language control for human motion synthesis. In *Computer Vision – ECCV 2024: 18th European Conference, Milan, Italy, September 29–October 4, 2024, Proceedings, Part XXXVII*, page 37–54, Berlin, Heidelberg, 2024. Springer-Verlag. [2](#), [3](#), [4](#), [7](#), [8](#)

[53] Haoru Wang, Wentao Zhu, Luyi Miao, Yishu Xu, Feng Gao, Qi Tian, and Yizhou Wang. Aligning motion generation with human perceptions. In *ICLR*, 2025. [7](#), [8](#)

[54] Yiming Xie, Varun Jampani, Lei Zhong, Deqing Sun, and Huaizu Jiang. Omnicontrol: Control any joint at any time for human motion generation. In *The Twelfth International Conference on Learning Representations*, 2024. [3](#), [4](#), [7](#)

[55] Sirui Xu, Zhengyuan Li, Yu-Xiong Wang, and Liang-Yan Gui. Interdiff: Generating 3d human-object interactions with physics-informed diffusion. In *ICCV*, 2023. [3](#)

[56] Jianrong Zhang, Yangsong Zhang, Xiaodong Cun, Shaoli Huang, Yong Zhang, Hongwei Zhao, Hongtao Lu, and Xi Shen. T2m-gpt: Generating human motion from textual descriptions with discrete representations. In *Proceedings of the IEEE/CVF Conference on Computer Vision and Pattern Recognition (CVPR)*, 2023. [3](#)

[57] Siwei Zhang, Bharat Lal Bhatnagar, Yuanlu Xu, Alexander Winkler, Petr Kadlecek, Siyu Tang, and Federica Bogo. Rohm: Robust human motion reconstruction via diffusion. In *CVPR*, 2024. [3](#), [4](#)

[58] Tianyi Zhang\*, Varsha Kishore\*, Felix Wu\*, Kilian Q. Weinberger, and Yoav Artzi. BERTScore: Evaluating text generation with BERT. In *ICLR*, 2020. [7](#), [1](#), [6](#)

[59] Xiaohan Zhang, Bharat Lal Bhatnagar, Vladimir Guzov, Sebastian Starke, and Gerard Pons-Moll. Couch: Towards controllable human-chair interactions. In *European Conference on Computer Vision (ECCV)*. Springer, 2022. [3](#)

[60] Yi Zhou, Connelly Barnes, Lu Jingwan, Yang Jimei, and Li Hao. On the continuity of rotation representations in neural networks. In *The IEEE Conference on Computer Vision and Pattern Recognition (CVPR)*, 2019. [4](#)

# FUSION: Full-Body Unified Motion Prior for Body and Hands via Diffusion

## Supplementary Material

### 7. Architecture

Figure 6 shows the model architecture of our motion prior. It is a transformer-based diffusion model with 19.7M trainable parameters.

### 8. Optimization Hyperparameters

Tab. 4 lists the optimization hyperparameters used in evaluation and ablation studies. The chosen configuration balances task compliance ( $\lambda_{\text{close}}$ ) with the plausibility of the resulting motion ( $\lambda_{\text{foot}}$ ,  $\lambda_{\text{ch}}$ ,  $\lambda_{\text{IK}}$ ).

Stage	Epoch	$\lambda_{\text{IK}}$	$\lambda_{\text{foot}}$	$\lambda_{\text{ch}}$	$\lambda_{\text{close}}$
1	800	0.5	0.5	0.5	1
2	800	0.1	0.1	0.1	1

Table 4. Optimization configuration. The same configuration applies across all ablation and evaluation settings.

### 9. Evaluation Metrics

Trajectory Error is the percentage of unsuccessful trajectories, defined as those with any keyframe location error exceeding a specified distance threshold. Location Error is the percentage of keyframe locations that exceed this threshold. Average Error measures the mean distance between the generated motion locations and the keyframe locations, measured at the keyframe motion steps.

### 10. Dataset Curation

Fig. 9 shows an example of random merging of the global body motion with local hand motion. Although it is rare, random merging of the local hand motion and the global body motion might introduce additional self-intersection. To address this issue, we perform a self-penetration test to ensure the obtained motions are physically possible. We compute face intersections between the hand mesh and the rest of the body mesh caused by copying the local hand motion. If there is an intersection exceeding a threshold, we discard this random merging in favor of another randomly sampled local hand motion.

### 11. Qualitative Results

For hand motion synthesis, we conducted a perceptual study comparing FUSION with both the GT and HMP [7] on the Keypoint Tracking task, which involves tracking all 10 fingertips on our test split. Participants were asked to evaluate the realism of motions involving the interaction of both hands with objects. Videos were presented side-by-side in

random order as shown in Fig. 10. Objects were included for visualization purposes only, to help users better distinguish between the motions. The evaluation criteria included hand jitter, naturalness of articulation, and object penetration. Subject preference ratios from 3 participants indicate that FUSION synthesizes more realistic hand motions than HMP and achieves a level of realism comparable to the Ground Truth. Fig. 10 shows the user panel.

### 12. Self-Interaction

We use our optimization framework with a prompted instance of GPT-o3 [30] to curate the self-interaction dataset. In total, there are 94 sequences with textual descriptions, contact conditions, and the corresponding human motions after optimization. This small dataset will be shared in the codebase.

#### 12.1. Sampling Body Vertices

We sample 236 vertices along with their semantic labels (*e.g.* `right_elbow_inside`, `left_biceps`) on the human body that may be important for self-interaction tasks. Figures 11 to 13 show the sampled vertices with a focus on the body, hands, and head, respectively.

#### 12.2. Quantitative Evaluation

Fig. 14 shows the devised pipeline for the evaluation of LLM planning. We run this all 94 every input sentence in our self-interaction. Tab. 5 shows every input–predicted sentence pair and the corresponding BERTScore values [58]. The last two rows are for the pairs with the highest and the lowest F1 score.

The BERTScore analysis of the input–predicted sentence pairs shows generally high alignment between the intended actions and their corresponding descriptions, with most F1 scores clustering above 0.85, indicating strong semantic similarity. Actions involving direct tactile interactions, such as *rubbing the palms together* (F1 = 0.953), *rub your left calf* (F1 = 0.962), and *smell your armpit* (F1 = 0.977), achieve particularly high scores, reflecting clear and unambiguous mappings between input and evaluation sentences. Gestures that are slightly more abstract or involve sequential motion, such as *do a squat* (F1 = 0.932) or *crossing arms* (F1 = 0.873), show slightly lower but still reasonable alignment. Overall, the table reflects that the predictions are semantically faithful to the inputs, with minor variations in descriptive richness or specificity influencing BERTScore variations.

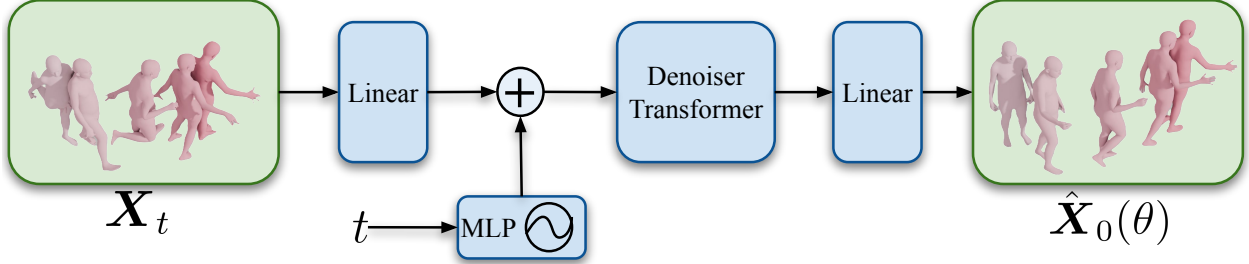


Figure 6. **FUSION Model Architecture**: Given a noisy motion  $\mathbf{X}_t$  and the corresponding noising timestep  $t$ , **FUSION** first performs linear projection, and concatenates it with the time embeddings of the noising timestep. This concatenation forms the input to the Denoiser Transformer. Then it performs linear projection to the Denoiser Transformer output and obtains denoised motion  $\hat{\mathbf{X}}_0(\theta)$ .

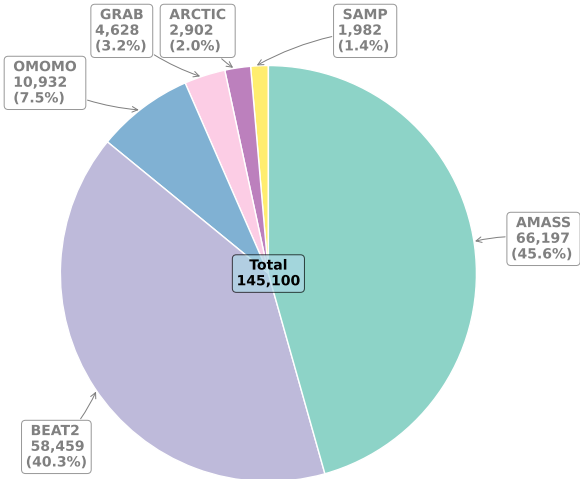


Figure 7. **Body Dataset Sequences**: Distribution of sequences across body motion datasets used for training. AMASS and BEAT2 constitute the majority of the training corpus, while smaller specialized datasets (OMOMO, GRAB, ARCTIC, and SAMP) provide additional diversity to the overall collection.

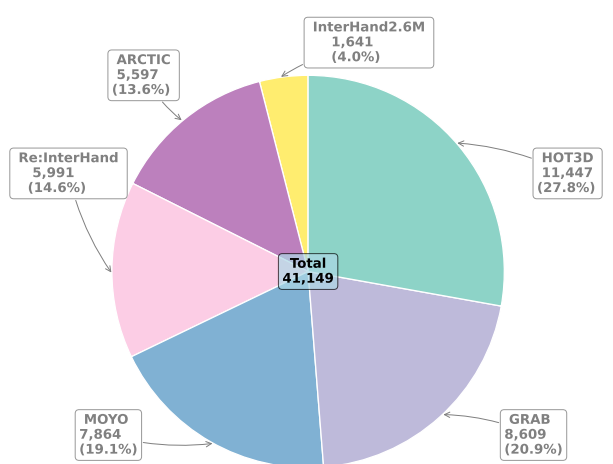


Figure 8. **Hand Dataset Sequences**: Distribution of sequences across hand motion datasets used for training. HOT3D constitutes the majority of the training corpus. GRAB, MOYO, Re:InterHand, ARCTIC, and InterHand2.6M datasets provide additional diversity to the overall collection.

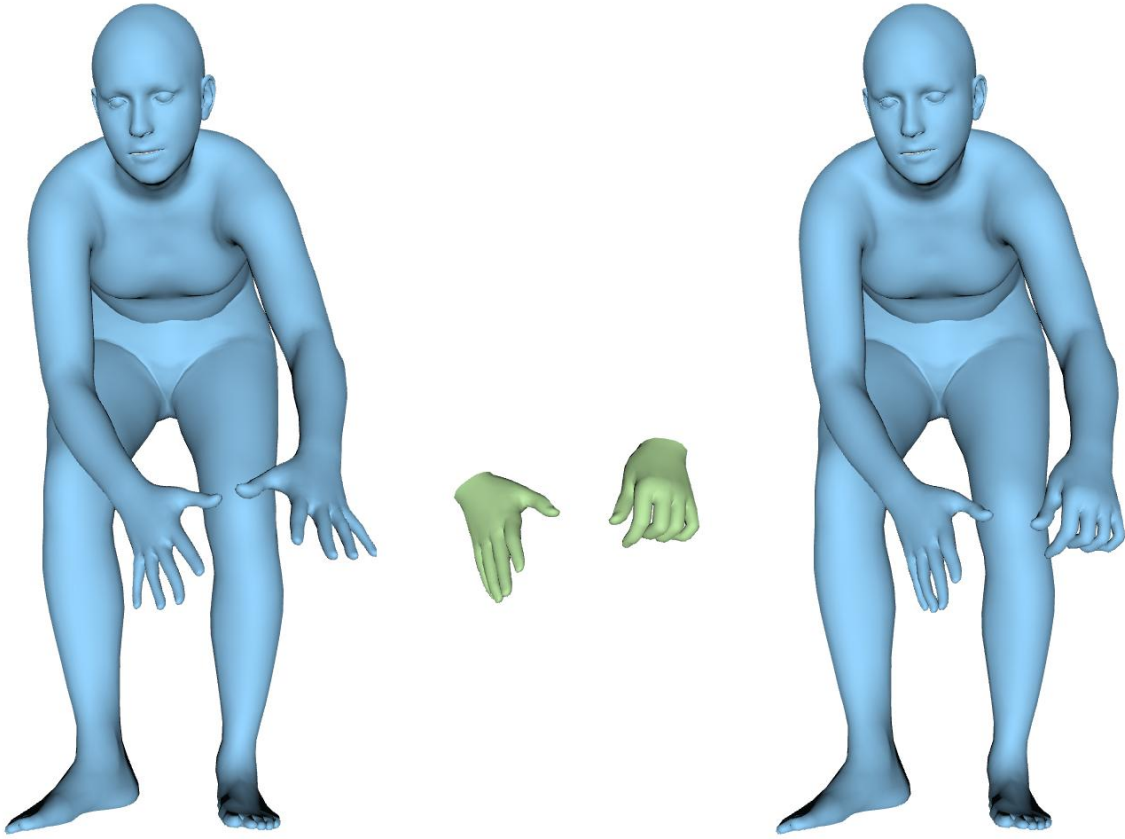


Figure 9. **FUSION Visualization of Random Body-Hand Pairing:** The mesh from the body dataset is shown on the left. The middle panel presents local hand meshes with randomly sampled poses, but with wrist orientations and locations taken from the GT data. On the right, we show the resulting full-body mesh obtained by combining the sampled hand poses with the corresponding body pose. Notably, self-penetration is effectively prevented, since the wrist orientations are directly derived from the body, ensuring consistent and plausible articulation.

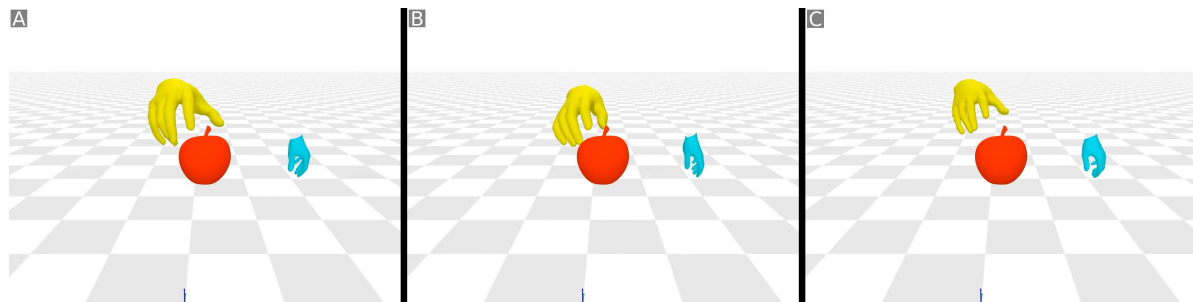
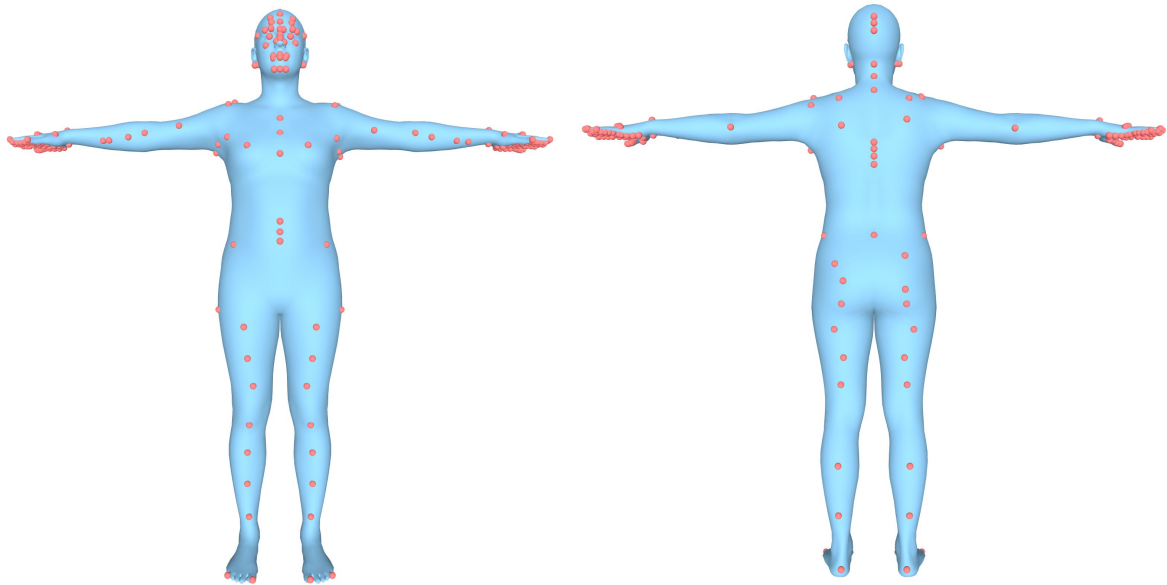


Figure 10. **User Study Graphical Interface:** Subjects were tasked with ranking the realism of the three options A, B, and C. Ordering is random for each interaction sample.



**Figure 11. Sampled vertices for the Self-Interaction Task:** We manually select 236 body vertices together with their semantic labels (e.g. *right\_fingertip*, *left\_biceps*, ...). The selected vertices are distributed across major body parts but are denser in the hands, as fine-grained hand articulations are more likely to come into contact during interaction. This manual selection ensures that the set covers contact-relevant regions, while keeping the number of vertices computationally manageable.

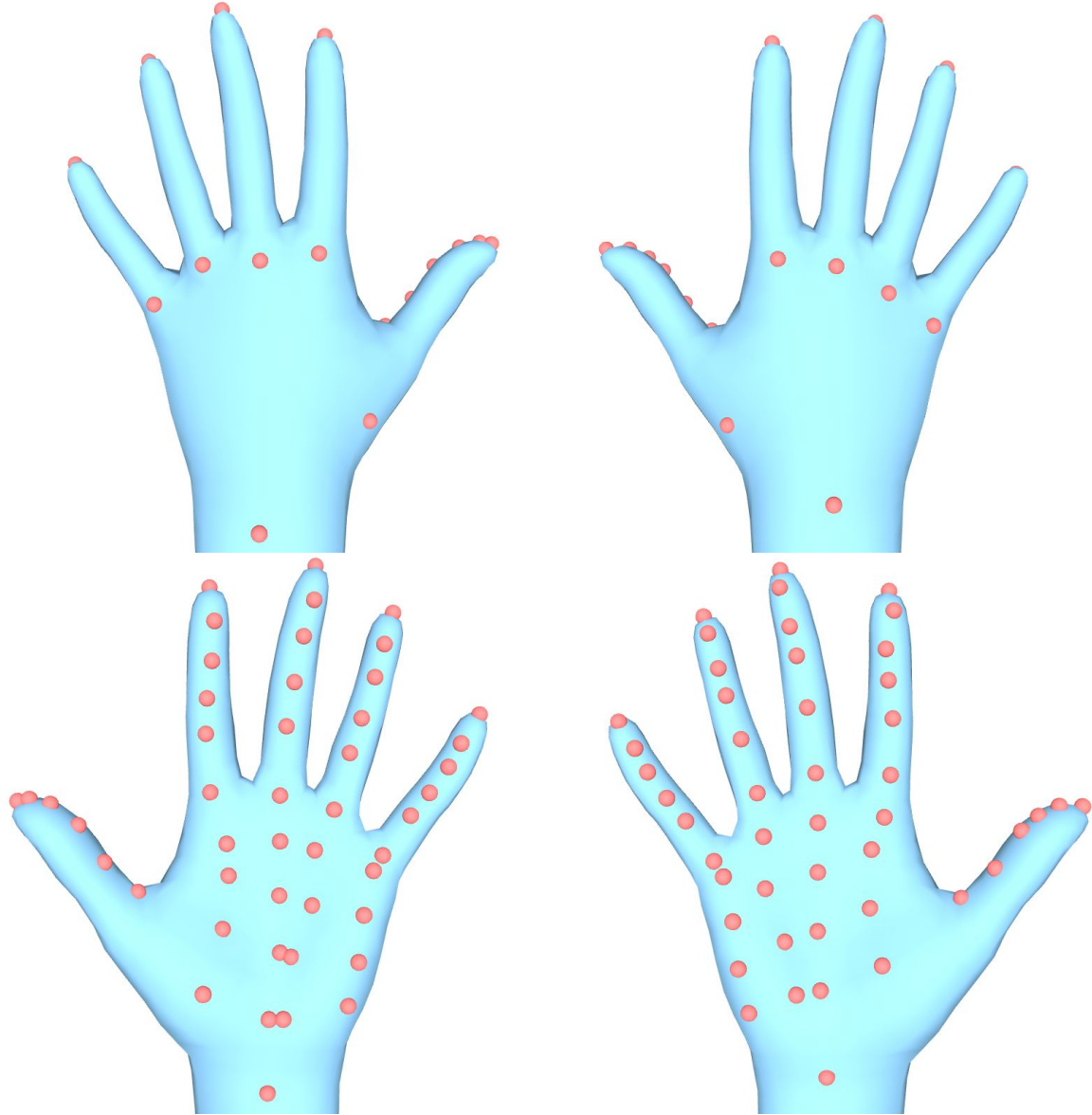


Figure 12. **Sampled hand vertices for the Self-Interaction Task:** The palms contain more sampled points than the back of hands to better capture contact in relevant tasks.

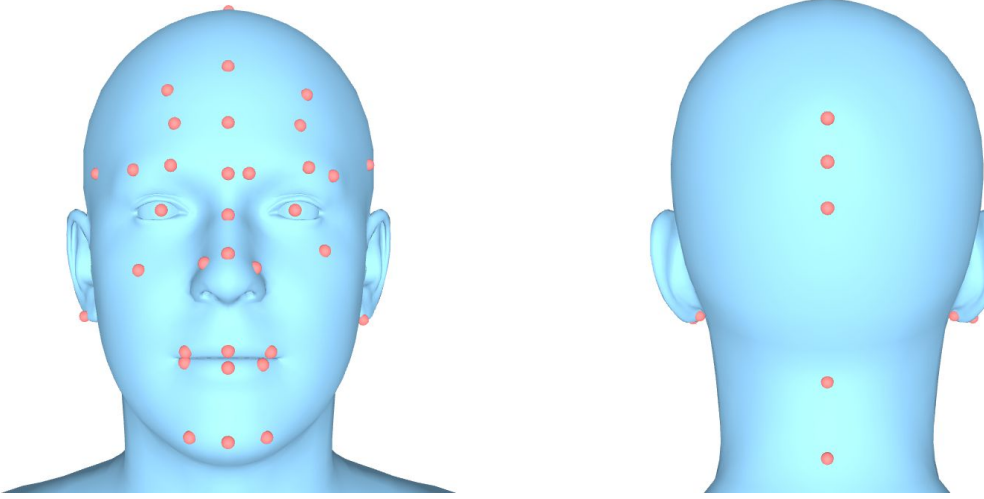


Figure 13. **Sampled head vertices for the Self-Interaction Task:** The face contains more sampled points than the back of the head to better capture contact in tasks such as touching the face.

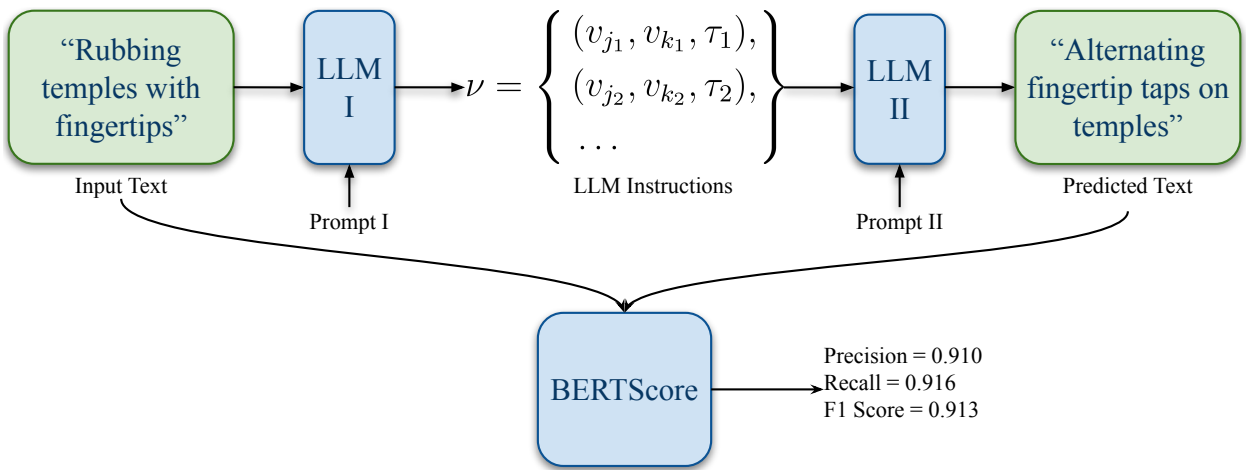


Figure 14. **Quantitative Analysis of LLM Outputs:** We employ a pipeline to verify the quality of LLM-generated plans. Specifically, we prompt a second instance of GPT-o3 with only four samples from the interaction dataset to generate a sentence describing the instruction. The second instance is then used in tandem with the first one to perform reverse reasoning. Then for each input–prediction sentence pair, BERT is used to compute precision, recall, and F1 score based on semantic similarity [58].

Index	Input Sentence	Evaluation Sentence	Precision	Recall	F1
1	Interlacing fingers	Press both palms and matching fingertips together in a prayer gesture.	0.862	0.852	0.857
2	Cracking knuckles	Slide your left thumb across the right knuckles, then press palms together.	0.842	0.859	0.85
3	Self fist bumping	Tap the knuckles of your hands together.	0.868	0.852	0.86
4	Rubbing the palms together	Rub your palms together.	0.954	0.952	0.953
5	Rubbing fingertips together	Alternately tap your left thumb with your index and middle fingertips.	0.854	0.885	0.869
6	Pressing thumb against palm	Slide your right thumb across your palm.	0.906	0.908	0.907
7	Rolling a ring around a finger	Rub your right ring finger with your thumb and middle fingertip.	0.862	0.9	0.881
8	Flicking one finger with another	Right-hand index taps between thumb and middle finger.	0.876	0.866	0.871
9	Massaging palm with opposite hand	Rub the left palm with the right thumb and index finger.	0.892	0.902	0.897
10	Tapping fingers against each other	Bring all corresponding fingertips of both hands together in a prayer-like touch.	0.86	0.875	0.867
11	Snap your fingers to make some noise	Snap your fingers with your right hand.	0.937	0.916	0.926
12	Pulling fingers one by one with the opposite hand	Right hand pinches each left fingertip in sequence.	0.884	0.891	0.887
13	Drumming left fingers on the back of the right hand	Tap your left fingertips on the knuckles of your right hand.	0.919	0.908	0.914
14	Tracing a circle or shape on the palm with a finger	Run your right index finger across your left palm.	0.889	0.881	0.885
15	Scratching forehead	Slide your left index finger across your forehead.	0.853	0.851	0.852
16	Rub your back of head	Scratch the back of your head with the left hand.	0.91	0.922	0.916
17	Tapping cheek with fingers	Touch your right cheek with your right fingertips.	0.896	0.911	0.903
18	Scratching chin or jawline	Thoughtful chin stroking.	0.88	0.86	0.87
19	Wiping sweat from forehead	Wipe your forehead with your right middle knuckle.	0.88	0.922	0.901
20	Resting fingertips against forehead	Touch your forehead with right fingertips.	0.918	0.921	0.92
21	Gently pinching and releasing fingers together	Do the OK gesture with the right hand.	0.883	0.854	0.868
22	Fixing hair	Slide right fingertips from temple over head to neck.	0.845	0.873	0.859
23	Touch you ear	Gently pinch your left earlobe.	0.881	0.907	0.894

Index	Input Sentence	Evaluation Sentence	Precision	Recall	F1
24	Grab your ear	Gently pinch your right earlobe with your right hand.	0.867	0.924	0.894
25	Cover both ears	Massage your earlobes with both palms.	0.881	0.912	0.896
26	Pinching own skin	Pinch your left forearm with your right thumb and index finger.	0.82	0.856	0.837
27	Adjusting glasses	Right hand pinches nose then earlobe.	0.859	0.862	0.861
28	Rubbing your knee	Stroke your left knee with your left hand.	0.871	0.904	0.887
29	Rub your left calf	Rub your left calf with your left hand.	0.945	0.98	0.962
30	Clapping hands twice	Rub your hands together.	0.921	0.893	0.907
31	Rubbing hands together	Rubbing palms together.	0.978	0.972	0.975
32	Grab your opposite ear	Pinch your right earlobe with the left hand.	0.891	0.921	0.905
33	Put your hands on your hips	Place your hands on your hips.	0.981	0.977	0.979
34	Both hands grabbing earlobes	Gently pinch both earlobes with thumb and index fingers.	0.882	0.912	0.897
35	Place your hands on your waists	Stand with hands on hips.	0.925	0.886	0.905
36	Fixing sleeves or rolling them up	Slide your right fingertips up your left arm.	0.861	0.86	0.86
37	Hands on knees to rest after running	Rest both palms on your knees.	0.898	0.882	0.89
38	Clean your armpit with your left hand	Scratch your left armpit with your left hand.	0.958	0.965	0.961
39	Scretch yourself by touching your toes	Slide your hands down your legs to touch your toes.	0.898	0.876	0.887
40	Touch your left heel with the left hand	Rub your left heel with your left hand.	0.971	0.972	0.971
41	Crossing arms and tapping arm with fingers	Lightly tap both biceps with opposite fingertips.	0.872	0.866	0.869
42	Placing both hands in front of the abdomen	Rest both hands on your belly.	0.935	0.919	0.927
43	Wrapping fingers around the opposite wrist	Hold your right wrist with your left hand.	0.887	0.902	0.894
44	Touching the back of the neck with one hand	Gently massage your neck with the left hand.	0.927	0.919	0.923
45	Secure your head in the moment of emergency	Scalp massage.	0.873	0.871	0.872
46	Pressing fingers against biceps or shoulders	Gently scratching left upper arm.	0.888	0.866	0.877
47	Scratching forearm or wrist with opposite fingers	Brush the left forearm with right fingertips.	0.914	0.891	0.902
48	One heel to the other knee	Rub your right shin with your left heel.	0.858	0.875	0.866
49	Running fingers across lips	Tap your lips with right index and middle fingers.	0.867	0.906	0.886
50	Fist bump your hands	Press your palms together in a prayer gesture.	0.884	0.869	0.877
51	Tracing a circle or shape on the palm with your thumb	Rub your left palm with your thumb.	0.935	0.9	0.917
52	Smell your armpit	Smell your right armpit.	0.97	0.984	0.977
53	Scratch your eyes with thumbs	Gently rub your eyes with both thumbs.	0.914	0.93	0.922
54	Gently pinching bridge of nose	Pinch your nose with the right hand.	0.917	0.89	0.903
55	Rubbing temples with fingertips	Alternating fingertip taps on temples.	0.91	0.916	0.913
56	Running ring and middle fingertips across lips	Slide right middle and ring fingertips across your lips.	0.919	0.942	0.93
57	Cover your mouth with your left hand over surprising news	Left hand gently touches chin and lips.	0.882	0.868	0.875
58	Kiss your hand palm	Wipe your lips with the right palm.	0.903	0.909	0.906

Index	Input Sentence	Evaluation Sentence	Precision	Recall	F1
59	Send a kiss to your valentine	Right-hand smoking gesture.	0.882	0.857	0.87
60	Crossing the arms over the chest	Cross arms over chest in a self-hug.	0.906	0.939	0.922
61	Resting hand on chin	Hold your chin with the right hand thoughtfully.	0.905	0.914	0.909
62	Stay in attention position	Stand with both palms on your back thighs, heels pressed together.	0.804	0.83	0.817
63	Clean your right armpit with your left hand	Scratch your right armpit with your left hand.	0.968	0.973	0.97
64	Tracing a shape on own forearm with the right index finger	Scratch your left forearm with your right index finger.	0.932	0.911	0.921
65	Making a 'spider walk' motion with index and middle fingertips on the opposite forearm	Scratch your left forearm with the right index and middle fingertips.	0.93	0.894	0.911
66	Do a squat	Do a deep squat, sitting on your heels.	0.899	0.969	0.932
67	Holding one wrist with the opposite hand	Right hand grasps left wrist.	0.915	0.91	0.912
68	Scratch your eyes	Rub your right eye with your right fingertips.	0.893	0.924	0.909
69	Blow nose with your right	Pinch your nose with your right hand.	0.935	0.931	0.933
70	Make delicious gesture	Blow a kiss with your right hand.	0.859	0.85	0.855
71	Crossing arms	Cross arms, fingertips resting on opposite biceps.	0.843	0.906	0.873
72	Scratching head	Gently scratch your head with right fingertips.	0.869	0.863	0.866
73	Holding stomach	Rest both hands on your belly.	0.871	0.885	0.878
74	Adjusting a tie	Touch chest with right fingertips.	0.875	0.871	0.873
75	Hugging yourself	Scratching your shoulder blades with both hands.	0.856	0.904	0.879
76	Gripping shoulder	Scratch left shoulder with right hand.	0.87	0.874	0.872
77	Tighten your belt	Gently touch belly and waist with both hands.	0.865	0.866	0.865
78	Salute a commander	Rub your right forehead with your right index and middle fingers.	0.811	0.849	0.83
79	Button your trousers	Pinch your lower abdomen using right thumb and index finger.	0.852	0.902	0.876
80	Adjusting a necklace	Straightening shirt collar with alternating hands.	0.87	0.909	0.889
81	Rub your outer elbow	Scratch left forearm.	0.904	0.88	0.892
82	Place hand over heart	Place right hand on chest.	0.942	0.936	0.939
83	Gently touch your back	Scratch your mid-back with your right hand.	0.91	0.916	0.913
84	Gently scratch your shin	Gently scratching right shin.	0.952	0.946	0.949
85	Adjusting a tie or necklace	Lightly tap up and down your sternum with right fingertips.	0.843	0.875	0.859
86	Running fingers along the arm	Run right fingertips down left arm.	0.909	0.939	0.924
87	Zipping or buttoning a jacket	Pinched right hand slides upward from belly to chest.	0.853	0.851	0.852
88	Brushing off dust from clothes	Slide your right fingertips across the chest.	0.874	0.85	0.862
89	Roll up both sleeves one by one	Gently stroke your opposite arms.	0.893	0.884	0.889
90	Trace a circle around your belly	Circle your navel with right index and middle fingertips.	0.857	0.917	0.886
91	Touching chin with the left hand	Rub your chin with left fingertips.	0.94	0.939	0.939
92	Rubbing belly with your left palm	Left-hand circular belly rub.	0.919	0.906	0.913
93	Clap your belly with your left hand	Left palm resting on stomach.	0.912	0.879	0.895
94	Resting one hand on the opposite shoulder	Left hand on right shoulder.	0.938	0.916	0.927

Index	Input Sentence	Evaluation Sentence	Precision	Recall	F1
62	Stay in attention position	Stand with both palms on your back thighs, heels pressed together.	0.804	0.83	0.817
33	Put your hands on your hips	Place your hands on your hips.	0.981	0.977	0.979

Table 5. **BERTScores for input–predicted sentence pairs**: Pairs with lowest and the highest scores shown in the last two rows. As seen in the figure the semantic similarity between input and predicted text pairs are high, indicating the effectiveness of the high-level LLM planning.